
Likelihood-Free Overcomplete ICA and Applications in Causal Discovery

Chenwei Ding

School of Computer Science
University of Sydney
cdin2224@uni.sydney.edu.au

Mingming Gong

School of Mathematics and Statistics
University of Melbourne
mingming.gong@unimelb.edu.au

Kun Zhang

Department of Philosophy
Carnegie Mellon University
kunz1@cmu.edu

Dacheng Tao

School of Computer Science
University of Sydney
dacheng.tao@uni.sydney.edu.au

Abstract

Causal discovery witnessed significant progress over the past decades. In particular, many recent causal discovery methods make use of independent, non-Gaussian noise to achieve identifiability of the causal models. Existence of hidden direct common causes, or confounders, generally makes causal discovery more difficult; whenever they are present, the corresponding causal discovery algorithms can be seen as extensions of overcomplete independent component analysis (OICA). However, existing OICA algorithms usually make strong parametric assumptions on the distribution of independent components, which may be violated on real data, leading to sub-optimal or even wrong solutions. In addition, existing OICA algorithms rely on the Expectation Maximization (EM) procedure that requires computationally expensive inference of the posterior distribution of independent components. To tackle these problems, we present a Likelihood-Free Overcomplete ICA algorithm (LFOICA¹) that estimates the mixing matrix directly by back-propagation without any explicit assumptions on the density function of independent components. Thanks to its computational efficiency, the proposed method makes a number of causal discovery procedures much more practically feasible. For illustrative purposes, we demonstrate the computational efficiency and efficacy of our method in two causal discovery tasks on both synthetic and real data.

1 Introduction

Discovering causal relations among variables has been an important problem in various fields such as medical science and social sciences. Because conducting randomized controlled trials is usually expensive or infeasible, discovering causal relations from observational data, *i.e.* causal discovery Pearl (2000); Spirtes et al. (2000)) has received much attention in the past decades. Classical causal discovery methods, such as PC Spirtes et al. (2000) and GES Chickering (2002), output

¹Code for LFOICA can be found [here](#)

multiple causal graphs in the Markov equivalence classes. Since the seminal work [Shimizu et al. \(2006\)](#), there have been various methods that have complete identifiability of the causal structure by making use of constrained Functional Causal Models (FCMs), such as linear non-Gaussian models [Shimizu et al. \(2006\)](#), nonlinear additive model [Hoyer et al. \(2009\)](#), and post-nonlinear model [Zhang and Hyvärinen \(2009\)](#).

Whenever there are essentially unobservable direct common causes of two variables (known as confounders), causal discovery can be viewed as learning with hidden variables. With the linearity and non-Gaussian noise constraints, it has been shown that the causal model is even identifiable from data with measurement error [Zhang et al. \(2018\)](#) or missing common causes [Hoyer et al. \(2008\)](#); [Geiger et al. \(2015\)](#); [Gong et al. \(2015, 2017\)](#); [Tank et al. \(2019\)](#). The corresponding causal discovery algorithms can be seen as extension of overcomplete independent component analysis (OICA). Unlike regular ICA [Hyvärinen et al. \(2004\)](#), in which the mixing matrix is invertible, OICA cannot utilize the change of variables technique to derive the joint probability density function of the data, which is a product of the densities of the independent components (ICs), divided by some value depending on the mixing matrix. The joint density immediately gives rise to the likelihood.

To perform maximum likelihood learning, existing OICA algorithms typically assume a parametric distribution for the hidden ICs. For example, if assuming each IC follows a Mixture of Gaussian (MoG) distribution, we can simply derive the likelihood for the observed data. However, the number of Gaussian mixtures increases exponentially in the number of ICs, which poses significant computational challenges. Many of existing OICA algorithms rely on the Expectation-Maximization (EM) procedure combined with approximate inference techniques, such as Gibbs sampling [Olshausen and Millman \(2000\)](#) and mean-field approximation [Højjen-Sørensen et al. \(2002\)](#), which usually sacrifice the estimation accuracy. Furthermore, the extended OICA algorithms for causal discovery are mostly noiseless OICA because they usually model all the noises as ICs [Zhang et al. \(2018\)](#); [Gong et al. \(2015\)](#). In order to apply EM, a very low variance Gaussian noise is usually added to the noiseless OICA model, resulting in very slow convergence [Petersen et al. \(2005\)](#). Finally, the parametric assumptions on the ICs might be restrictive for many real-world applications.

To tackle these problems, we propose a Likelihood-Free OICA (LFOICA) algorithm that makes no explicit assumptions on the density functions of the ICs. In light of recent work on adversarial learning [Goodfellow et al. \(2014\)](#), LFOICA utilizes neural networks to learn the distribution of independent components implicitly. By minimizing appropriate distributional distance between the generated data from LFOICA model and the observed data, all parameters including the mixing matrix and noise learning network parameters in LFOICA can be estimated very efficiently via stochastic gradient descent (SGD) [Kingma and Ba \(2014\)](#); [Duchi et al. \(2011\)](#), without the need to formulate the likelihood function. The proposed LFOICA will make a number of causal discovery procedures much more practically feasible. For illustrative purposes, we extend our LFOICA method to tackle two causal discovery tasks, including causal discovery from data with measurement noise [Zhang et al. \(2018\)](#) and causal discovery from low-resolution time series [Gong et al. \(2015, 2017\)](#). Experimental results on both synthetic and real data demonstrate the efficacy and efficiency of our proposed method.

2 Likelihood-Free Over-complete ICA

2.1 General Framework

Linear ICA assumes the following data generation model:

$$\mathbf{x} = \mathbf{A}\mathbf{s}, \tag{1}$$

where $\mathbf{x} \in \mathbb{R}^p$, $\mathbf{s} \in \mathbb{R}^d$, $\mathbf{A} \in \mathbb{R}^{p \times d}$ are known as mixtures, independent components (ICs), and mixing matrix respectively. The elements in \mathbf{s} are supposed to be independent from each other and each follows a non-Gaussian distribution (or at most one of them is Gaussian). The goal of ICA is to recover both \mathbf{A} and \mathbf{s} from observed mixtures \mathbf{x} . However, in the context of causal discovery, our main goal is to recover a constrained \mathbf{A} matrix. When $d > p$, the problem is known as overcomplete ICA (OICA).

In light of recent advances in Generative Adversarial Nets (GANs) [Goodfellow et al. \(2014\)](#), we propose to learn the mixing matrix in the OICA model by designing a generator that allows us to

draw samples easily. We model the distribution of each source s_i by a function model f_{θ_i} that transforms a Gaussian variable z_i to the non-Gaussian source. More specifically, the i -th source can be generated by $\hat{s}_i = f_{\theta_i}(z_i)$, where $z_i \sim \mathcal{N}(0, 1)$. Thus, the whole generator that generate \mathbf{x} can be written as

$$\hat{\mathbf{x}} = \mathbf{A}[\hat{s}_1, \dots, \hat{s}_d]^\top = \mathbf{A}[f_{\theta_1}(z_1), \dots, f_{\theta_d}(z_d)]^\top = G_{\mathbf{A}, \boldsymbol{\theta}}(\mathbf{z}), \quad (2)$$

where $\boldsymbol{\theta} = [\theta_1, \dots, \theta_d]^\top$ and $\mathbf{z} = [z_1, \dots, z_d]^\top$. Figure 1 shows the graphical structure of our LFOICA generator $G_{\mathbf{A}, \boldsymbol{\theta}}$ with 4 sources and 3 mixtures. We use a multi-layer perceptron (MLP) to model each f_{θ_i} . While most of the previous algorithms for both undercomplete Hyvarinen (1999); Brakel and Bengio (2017); Amari et al. (1996); Hyvärinen and Oja (2000) and overcomplete Le et al. (2011) scenarios try to minimized the dependence among the recovered components, the components \hat{s}_i recovered by LFOICA are essentially independent because the noises z_i are independent, according to the generating process.

The LFOICA generator $G_{\mathbf{A}, \boldsymbol{\theta}}$ can be learned by minimizing the distributional distance between the data sampled from the generator and the observed \mathbf{x} data. Various distributional distances have been applied in training generative networks, including the Jensen-Shannon divergence Goodfellow et al. (2014), Wasserstein distance Arjovsky et al. (2017), and Maximum Mean Discrepancy (MMD) Li et al. (2015); Gretton et al. (2012). Here we adopt MMD as the distributional distance as it does not require an explicit discriminator network, which simplifies the whole optimization procedure. Specifically, we learn the parameters $\boldsymbol{\theta}$ and \mathbf{A} in the generator by solving the following optimization problem:

$$\begin{aligned} \mathbf{A}^*, \boldsymbol{\theta}^* &= \arg \min_{\mathbf{A}, \boldsymbol{\theta}} M(\mathbb{P}(\mathbf{x}), \mathbb{P}(G_{\mathbf{A}, \boldsymbol{\theta}}(\mathbf{z}))) \\ &= \arg \min_{\mathbf{A}, \boldsymbol{\theta}} \left\| \mathbb{E}_{\mathbf{x} \sim p(\mathbf{x})}[\phi(\mathbf{x})] - \mathbb{E}_{\mathbf{z} \sim p(\mathbf{z})}[\phi(G_{\mathbf{A}, \boldsymbol{\theta}}(\mathbf{z}))] \right\|^2, \end{aligned} \quad (3)$$

where ϕ is the feature map of a kernel function $k(\cdot, \cdot)$. MMD can be calculated by using kernel trick without the need for an explicit ϕ . By choosing characteristic kernels, such as Gaussian kernel, MMD is guaranteed to match the distributions Sriperumbudur et al. (2011). In practice, we optimize some empirical estimator of (3) on minibatches by stochastic gradient descent (SGD). The entire procedure is shown in Algorithm 1.

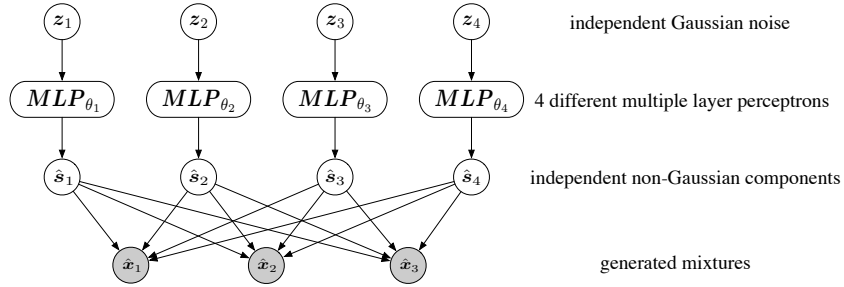


Figure 1: generator architecture of LFOICA. z_1, z_2, z_3, z_4 are i.i.d Gaussian noise variables.

It has been proved that under some assumptions including the non-Gaussian assumption, the mixing matrix \mathbf{A} can be estimated up to permutation and scaling indeterminacies (including the sign indeterminacy) of the columns Eriksson and Koivunen (2004). Our LFOICA matches the distributions of generated and real data, although not via maximum likelihood estimation, and the previous identifiability result applies. It is worth noting that although the parameters of the MLPs are unidentifiable, the learned noise distribution and mixing matrix are identifiable up to scale and permutation indeterminacies under appropriate assumptions.

2.2 Practical Considerations

We consider two important issues when applying LFOICA to real applications.

Sparsity Based on the fact that the mixing matrix is sparse in many real systems, we add a LASSO regularizer Tibshirani (1996) to (3), resulting in the loss function $M(\mathbb{P}(\mathbf{x}), \mathbb{P}(G_{\mathbf{A}, \boldsymbol{\theta}}(\mathbf{z}))) +$

Algorithm 1 Likelihood-Free Overcomplete ICA (LFOICA) Algorithm

- 1: Get a minibatch of i.i.d samples \mathbf{z} from Gaussian noise distribution.
 - 2: Generate mixtures using (2).
 - 3: Get a minibatch of samples from the distribution of observed mixtures $p(\mathbf{x})$.
 - 4: Update \mathbf{A} and θ by minimizing the empirical estimate of (3) on the minibatch.
 - 5: Repeat step 1 to step 4 until max iterations reached.
-

$\lambda \sum_i \sum_j |\mathbf{A}_{ij}|$. We use the stochastic proximal gradient method [Nitanda \(2014\)](#) to train our model. The proximal mapping for LASSO regularizer corresponds to the soft-thresholding operator:

$$\text{prox}_\gamma(\mathbf{A}) = S_{\lambda\gamma}(\mathbf{A}) = \begin{cases} \mathbf{A} - \lambda\gamma & \text{if } \mathbf{A} > \lambda\gamma \\ 0 & \text{if } -\lambda\gamma \leq \mathbf{A} \leq \lambda\gamma \\ \mathbf{A} + \lambda\gamma & \text{if } \mathbf{A} < -\lambda\gamma \end{cases},$$

where λ, γ are the regularization weight and the learning rate, respectively. The soft-thresholding operator is applied after each gradient descent step:

$$\mathbf{A}^{(t)} = \text{prox}_{\lambda\gamma_t} \left(\mathbf{A}^{(t-1)} - \gamma_t \nabla M_{\mathbf{A}^{(t-1)}}(\cdot) \right), \quad t = 1, 2, 3, \dots$$

Insufficient data When we have rather small datasets, it is beneficial to have certain “parametric” assumptions on the source distributions. Here we use Mixture of Gaussian (MoG) distribution to model the non-Gaussian distribution of independent components. Specifically, the distribution for the i -th IC is

$$p_{\hat{s}_i} = \sum_{j=1}^m P(z_i = j) P(\hat{s}_i | z_i = j) = \sum_{j=1}^m w_{i,j} \mathcal{N}(\hat{s}_i | \mu_{i,j}, \sigma_{i,j}^2), \quad i = 1, 2, \dots, d,$$

where m is the number of Gaussian components in MoG and w_{ij} is the mixture proportions satisfying $\sum_{j=1}^m w_{ij} = 1$. If we do not wish to learn w_{ij} , we can first sample z_i from the categorical distribution $P(z_i = j) = w_{ij}$, and then use the reparameterization trick in [Kingma and Welling \(2013\)](#) to sample from $P(\hat{s}_i | z_i)$ by an encoder network $\hat{s}_i = \mu_{i,z_i} + \epsilon \sigma_{i,z_i}$, where $\epsilon \sim \mathcal{N}(0, 1)$. In this way, the gradients can be backpropagated to μ_{ij} and σ_{ij} . Learning w_{ij} is relatively hard because z_i is discrete and thus does not allow for backpropagation to w_{ij} . To address this problem, we adopt the Gumbel-softmax trick [Jang et al. \(2016\)](#); [Maddison et al. \(2017\)](#) to sample z_i . Specifically, we use the following softmax function to generate one-hot $\tilde{\mathbf{z}}_i$:

$$\tilde{z}_{ij} = \frac{\exp((\log(w_{ij}) + g_j) / \tau)}{\sum_{k=1}^m \exp((\log(w_{ik}) + g_k) / \tau)}, \quad (4)$$

where g_1, \dots, g_m are i.i.d samples drawn from Gumbel(0,1), and τ is the temperature parameter that controls the approximation accuracy of softmax to argmax. By leveraging the two tricks, we can sample \hat{s}_i from the generator $\hat{s}_i = \mathbf{u}\tilde{\mathbf{z}}_i + \epsilon\mathbf{v}\tilde{\mathbf{z}}_i$, where $\mathbf{u} = [\mu_{i1}, \dots, \mu_{im}]$ and $\mathbf{v} = [\sigma_{i1}, \dots, \sigma_{im}]$, which enables learning of all the parameters in the MoG model.

3 Applications in Causal Discovery

3.1 Causal Discovery under Measurement Error

Measurement error (e.g., noise caused by sensors) in the observed data can lead to wrong result of various causal discovery methods. Recently, it was proven that the causal structure is identifiable from data with measurement error, under the assumption of linear relations and non-Gaussian noise [Zhang et al. \(2018\)](#). Based on the identifiability theory in [Zhang et al. \(2018\)](#), we propose a causal discovery algorithm by extending LFOICA with additional constraints.

Following [Zhang et al. \(2018\)](#), we use the LiNGAM model [Shimizu et al. \(2006\)](#) to represent the causal relations on the data without measurement error. More specifically, the causal model is $\tilde{\mathbf{X}} = \mathbf{B}\tilde{\mathbf{X}} + \tilde{\mathbf{E}}$, where $\tilde{\mathbf{X}}$ is the vector of the variables without measurement error, $\tilde{\mathbf{E}}$ is the vector of independent non-Gaussian noise terms, and \mathbf{B} is the corresponding causal adjacency matrix in which B_{ij} is the coefficient of the direct causal influence from \tilde{X}_j to \tilde{X}_i and $B_{ii} = 0$ (no self-influence).

In fact, $\tilde{\mathbf{X}}$ is a linear transformation of the noise term $\tilde{\mathbf{E}}$ because the linear model can be rewritten as $\tilde{\mathbf{X}} = (\mathbf{I} - \mathbf{B})^{-1}\tilde{\mathbf{E}}$. Then, the model with measurement error \mathbf{E} can be written as

$$\mathbf{X} = \tilde{\mathbf{X}} + \mathbf{E} = (\mathbf{I} - \mathbf{B})^{-1}\tilde{\mathbf{E}} + \mathbf{E} = [(\mathbf{I} - \mathbf{B})^{-1} \quad \mathbf{I}] \begin{bmatrix} \tilde{\mathbf{E}} \\ \mathbf{E} \end{bmatrix}, \quad (5)$$

where \mathbf{X} is the vector of observable variables, and \mathbf{E} the vector of measurement error terms. Obviously, (5) is a special OCIA model with $[(\mathbf{I} - \mathbf{B})^{-1} \quad \mathbf{I}]$ as the mixing matrix. Therefore, we can readily extend our LFOICA algorithm to estimate the causal adjacency matrix \mathbf{B} .

3.2 Causal Discovery from Subsampled Time Series

Granger causal analysis has been shown to be sensitive to temporal frequency/resolution of time series. If the temporal frequency is lower than the underlying causal frequency, it is generally difficult to discover the high-frequency causal relations. Recently, it has been shown that the high-frequency causal relations are identifiable from subsampled low-frequency time series under the linearity and non-Gaussianity assumptions [Gong et al. \(2015\)](#). The corresponding model can also be viewed as extensions of OICA and the model parameters are estimated in the (variational) Expectation Maximization framework [Gong et al. \(2015\)](#). However, with the non-Gaussian ICs, *e.g.*, MoG is used in [Gong et al. \(2015\)](#), the EM algorithm is generally intractable while the variational EM algorithm loses accuracy. To make causal discovery from subsampled time series practically feasible, we further extend our LFOICA to discover causal relations from such data.

Following [Gong et al. \(2015\)](#), we assume that data at the original causal frequency follow a first-order vector autoregressive process (VAR(1)):

$$\mathbf{x}_t = \mathbf{C}\mathbf{x}_{t-1} + \mathbf{e}_t, \quad (6)$$

where $\mathbf{x}_t \in \mathbb{R}^n$ is the high frequency data and $\mathbf{e}_t \in \mathbb{R}^n$ represents independent non-Gaussian noise in the causal system. $\mathbf{C} \in \mathbb{R}^{n \times n}$ is the causal transition matrix at true causal frequency with C_{ij} representing the temporal causal influence from variable j to variable i . As done in [Gong et al. \(2015\)](#), we consider the following subsampling scheme under which the low frequency data can be obtained: for every k consecutive data points, one is kept and the others being dropped. Then the observed subsampled data with subsampling factor k admits the following representation [Gong et al. \(2015\)](#):

$$\tilde{\mathbf{x}}_{t+1} = \mathbf{C}^k \tilde{\mathbf{x}}_t + \mathbf{L}\tilde{\mathbf{e}}_{t+1}, \quad (7)$$

where $\tilde{\mathbf{x}}_t \in \mathbb{R}^n$ is the observed data subsampled from \mathbf{x}_t , $\mathbf{L} = [\mathbf{I}, \mathbf{C}, \mathbf{C}^2, \dots, \mathbf{C}^{k-1}]$, and $\tilde{\mathbf{e}}_t = (\mathbf{e}_{1+tk-0}^\top, \mathbf{e}_{1+tk-1}^\top, \dots, \mathbf{e}_{1+tk-(k-1)}^\top)^\top \in \mathbb{R}^{nk}$ is a vector containing nk independent noise terms. We are interested in estimating the transition matrix \mathbf{C} from the subsampled data. A graphical representation of the subsampled data is given in Figure 2(a). Apparently, (7) extends the OICA model by considering temporal relations between observed $\tilde{\mathbf{x}}_t$.

To apply our LFOICA to this problem, we propose to model the conditional distribution $\mathbb{P}(\tilde{\mathbf{x}}_{t+1}|\tilde{\mathbf{x}}_t)$ using the following model:

$$\hat{\tilde{\mathbf{x}}}_{t+1} = G_{\mathbf{C}, \theta}(\tilde{\mathbf{x}}_t, \mathbf{z}_{t+1}) = \mathbf{C}^k \tilde{\mathbf{x}}_t + \mathbf{L}[f_{\theta_1}(z_{t+1,1}), \dots, f_{\theta_{nk}}(z_{t+1,nk})]^\top, \quad (8)$$

which belongs to the broad class of conditional Generative Adversarial Nets (cGANs) [Mirza and Osindero \(2014\)](#). We call this extension of LFOICA as LFOICA-conditional. A graphical representation of (8) is shown in Figure 2(b). To learn the parameters in (8), we minimize the MMD between the joint distributions of true and generated data:

$$\begin{aligned} \mathbf{C}^*, \theta^* &= \arg \min_{\mathbf{C}, \theta} M(\mathbb{P}(\tilde{\mathbf{x}}_t, \tilde{\mathbf{x}}_{t+1}), \mathbb{P}(G_{\mathbf{C}, \theta}(\tilde{\mathbf{x}}_t, \mathbf{z}_{t+1}), \tilde{\mathbf{x}}_{t+1})) \\ &= \arg \min_{\mathbf{C}, \theta} \left\| \mathbb{E}_{(\tilde{\mathbf{x}}_t, \tilde{\mathbf{x}}_{t+1}) \sim p(\tilde{\mathbf{x}}_t, \tilde{\mathbf{x}}_{t+1})} [\phi(\tilde{\mathbf{x}}_t) \otimes \phi(\tilde{\mathbf{x}}_{t+1})] \right. \\ &\quad \left. - \mathbb{E}_{\tilde{\mathbf{x}}_t \sim p(\tilde{\mathbf{x}}_t), \mathbf{z}_{t+1} \sim p(\mathbf{z}_{t+1})} [\phi(\tilde{\mathbf{x}}_t) \otimes \phi(G_{\mathbf{C}, \theta}(\mathbf{z}_{t+1}))] \right\|^2, \end{aligned} \quad (9)$$

where \otimes denotes tensor product. The empirical estimate of (9) can be obtained by randomly sampling $(\tilde{\mathbf{x}}_t, \tilde{\mathbf{x}}_{t+1})$ pairs from true data and sampling from $\mathbb{P}(\mathbf{z}_{t+1})$. Again, we can use the mini-batch SGD algorithm to learn the model parameters efficiently.

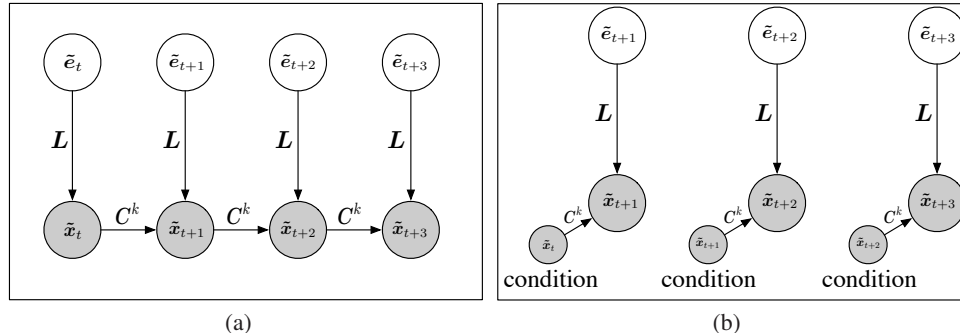


Figure 2: (a) Subsampled data with subsampling factor k . (b) LFOICA-conditional model for subsampled data.

4 Experiment

In this section, we conduct empirical studies on both synthetic and real data to show the effectiveness of our LFOICA algorithm and its extensions to solve causal discovery problems. We first compare the results obtained by LFOICA and several OICA algorithms on synthetic over-complete mixtures data. Then we apply the extensions of LFOICA mentioned in Section 3.1 and 3.2 in two causal discovery problems using both synthetic and real data.

4.1 Recovering Mixing Matrix from Synthetic OICA Data

We compare LFOICA with several well-known OICA algorithms on synthetic OICA data.

According to Eriksson and Koivunen (2004), the mixing matrix in OICA can be estimated up to the permutation and scaling indeterminacies (including the sign indeterminacy) of the columns. However, these indeterminacies stop us from comparing the estimated mixing matrices by different OICA algorithms. In order to make the comparison achievable, we need to eliminate these indeterminacies. To eliminate the permutation indeterminacy, we make the non-Gaussian distribution for each synthetic IC not only independent, but also different. With different distributions for each IC, it is convenient to permute the columns to the same order for all the algorithms according to the recovered distribution of each IC. We use Laplace distributions with different variance for each IC. In order to eliminate the scaling indeterminacy, both ground-truth and estimated mixing matrix are normalized to make the L2 norm of the first column equal to 1. With the permutation and scaling indeterminacy eliminated, we can conveniently compare the mixing matrices obtained by different algorithms. To further avoid local optimum, the mixing matrix is initialized by its true value added with large noise.

Table 1 compares the mean square error (MSE) between the ground-truth mixing matrix used to generate the data and the estimated mixing matrices by different OICA algorithms. In the table, RICA represents reconstruction ICA Le et al. (2011), MFICA_Gauss and MFICA_MoG represents mean-field ICA Højjen-Sørensen et al. (2002) with the prior distribution of ICs set to the Gaussian and the mixture of Gaussians respectively. NG-EM denotes the EM-based ICA Gong et al. (2015). p is the number of mixtures, and d is the number of ICs. For each algorithm, we conduct experiments in 4 cases (with $[p = 2, d = 4]$, $[p = 3, d = 6]$, $[p = 4, d = 8]$, and $[p = 5, d = 10]$). Each experiment is repeated 10 times with randomly generated data and the results are averaged. As we can see, our LFOICA achieves best result (smallest error) compared with the others. We also compare the distribution of the recovered components by LFOICA with the ground-truth, the result can be found in Section 1.2 of Supplementary Material.

4.2 Recovering Causal Relation from Causal Model with Measurement Error

Synthetic Data We generate data with measurement error, and the details about the generating process can be found in section 2.1 of Supplementary Material. NG-EM Gong et al. (2015) is a causal discovery algorithm as an extension of EM-based OICA method. Table 2 compares the MSE between the ground-truth causal adjacency matrix and those estimated by NG-EM and our LFOICA.

Table 1: MSE of the recovered mixing matrix by different methods on synthetic OICA data.

Methods	p=2, d=4	p=3, d=6	p=4, d=8	p=5, d=10
RICA	2.26e-2	1.54e-2	9.03e-3	7.54e-3
MFICA_Gauss	4.54e-2	2.45e-2	4.21e-2	3.18e-2
MFICA_MoG	2.38e-2	9.17e-3	2.43e-2	1.04e-2
NG-EM	1.82e-2	6.56e-3	1.21e-2	6.34e-3
LFOICA	4.61e-3	5.95e-3	6.96e-3	5.92e-3

Table 2: MSE of the recovered causal adjacency matrix by LFOICA and NG-EM.

Methods	MSE			Time (seconds)		
	n=5	n=7	n=50	n=5	n=7	n=50
LFOICA	1.04e-3	5.79e-3	1.81e-2	75.01	76.44	1219.34
NG-EM	6.98e-3	9.85e-3	-	1826.60	4032.54	-

The synthetic data we used contains 5000 data points. We test 3 cases where the number of variables n is 5, 10, and 50 respectively. Each experiment is repeated 10 times with random generated data and the results are averaged. As we can see from the table, LFOICA performs better than NG-EM, with smaller estimation error. We also compare the time taken by the two methods with the same number of iterations. As can be seen, NG-EM is much more time consuming than LFOICA (because EM needs to calculate the posterior). We found that when $n > 7$, NG-EM fails to obtain any results because it runs out of memory, while LFOICA can still obtain reasonable result. So no results of NG-EM is given in the table for $n = 50$. These experiments show that besides the efficacy, LFOICA is computationally much more efficient and uses less space than NG-EM as well.

Real Data We apply LFOICA to Sachs’s data [Sachs et al. \(2005\)](#) with 11 variables. Sachs’s data is a record of various cellular protein concentrations under a variety of exogenous chemical inputs and, inevitably, one can imagine that there is much measurement error in the data because of the measuring process. Here we visualize the causal diagram estimated by LFOICA and the ground-truth in Figure 3(a) and 3(d). The estimated causal adjacency matrix by LFOICA can be found in section 2.2 of Supplementary Material. For comparison, we also visualize the causal diagrams estimated by NG-EM and the corresponding ground-truth in Figure 3(b) and 3(e). To demonstrate the fact that regular causal discovery algorithm cannot properly estimate the underlying causal relations under measurement error, we further compare the result by a regular causal discovery algorithm called Linear, Non-Gaussian Model (LiNG) [Lacerda et al. \(2012\)](#) in Figure 3(c). Unlike LiNGAM, LiNG allows feedback in the causal model. We calculate the precision and recall for the output of the three algorithms. The precision are 51.22%, 48.94% and 50.00% for LFOICA, NG-EM and LiNG, and the recall are 55.26%, 60.53% and 23.68% respectively. As we can see, LiNG fails to recover most of the causal directions while LFOICA and NG-EM perform clearly better. This makes an important point that measurement error can lead to misleading results by regular causal discovery algorithms, while OICA-based algorithms such as LFOICA and NG-EM are able to produce better results. Although the performances of LFOICA and NG-EM are very close, it takes about 48 hours for NG-EM to obtain the result while LFOICA takes only 142.19s, which further demonstrates the remarkable computational efficiency of LFOICA.

4.3 Recovering Causal Relation from Low-Resolution Time Series Data

We then consider discovery of time-delayed causal relations at the original high frequency (represented by the VAR model) from their subsampled time series. We conduct experiments on both synthetic and real data.

Synthetic Data Following [Gong et al. \(2015\)](#), we generate synthetic time series data at the original causal frequency using VAR(1) model described by (6). Details about how the data is generated can be found in section 3.1 of Supplementary Material. NG-EM and NG-MF were first proposed in [Gong et al. \(2015\)](#) as extensions of OICA algorithms to discover causal relation from low-resolution

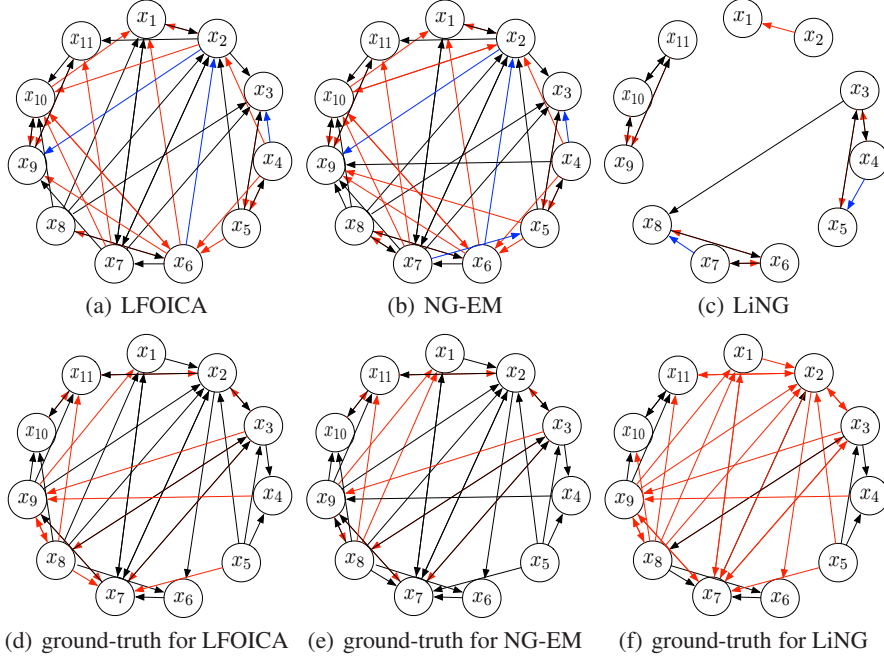


Figure 3: (a)-(c) Causal diagrams by LFOICA, NG-EM and LiNG. (d)-(f) Three ground-truth causal diagrams which are actually the same with the red arrows representing the missing causal directions in the output of the corresponding algorithm. The red arrows in (a)-(c) are falsely discovered causal directions compared with ground-truth. The blue arrows in (a)-(c) are edges with converse causal directions compared with ground-truth.

Table 3: MSE of the recovered transition matrix by different methods on synthetic subsampled data.

Methods	n=2							
	T=100				T=300			
	k=2	k=3	k=4	k=5	k=2	k=3	k=4	k=5
LFOICA-conditional	7.25e-3	7.88e-3	8.45e-3	9.00e-3	1.12e-3	3.87e-3	4.07e-3	6.23e-3
NG-EM	6.50e-3	7.32e-3	1.02e-2	1.04e-2	7.24e-3	9.11e-3	9.54e-3	9.98e-3
NG-MF	9.09e-3	9.89e-3	1.24e-2	2.19e-2	8.46e-3	8.76e-3	1.01e-2	2.20e-2

data. Table 3 shows the MSE between the ground-truth transition matrix and those estimated by LFOICA-conditional, NG-EM, and NG-MF when number of variables $n = 2$. We conduct experiments when the subsampling factor is set to $k = 2, 3, 4, 5$ and size of dataset $T = 100$ and 300 . Each experiment is repeated 10 random replications and the results are averaged. As one can see from Table 3, LFOICA-conditional achieves comparable result as NG-EM and NG-MF [Gong et al. \(2015\)](#). NG-EM has better performance when the number of data points is small ($T = 100$), probably because the MMD distance measure used in LFOICA-conditional may be inaccurate with small number of samples. When the number of data points is larger ($T = 300$), LFOICA-conditional obtains the best results. We also conduct experiment when n is larger ($n = 5$). The result can be found in Section 3.2 of Supplementary Material; again, LFOICA-conditional gives more accurate results and it is computationally much more efficient.

Real Data Here we use [Temperature Ozone Data Mooij et al. \(2016\)](#), which corresponds to the 49th, 50th, and 51st causal-effect pairs in the database. These three temperature ozone pairs are taken at three different places in 2009. Each pair of data contains two variables, ozone and temperature, with the ground-truth causal direction temperature \rightarrow ozone. To demonstrate the result when $n = 2$, we use the 50th pair as in [Gong et al. \(2015\)](#). The optimal subsampling factor k can be determined using the method of cross-validation on the log-likelihood of the models. Here we use

$k = 2$ according to [Gong et al. \(2015\)](#). The estimated transition matrix $\mathbf{C} = \begin{bmatrix} 0.9310 & 0.1295 \\ -0.0017 & 0.9996 \end{bmatrix}$ (the first variable is ozone and the second is temperature in the matrix). from which we can clearly find the causal direction from temperature to ozone. We also conduct experiments when $n = 6$. The result can be found in section 3.3 in Supplementary Material.

5 Conclusion

In this paper, we proposed a Likelihood-Free Overcomplete ICA model (LFOICA), which does not require parametric assumptions on the distributions of the independent sources. By generating the sources using neural networks and directly matching the generated data and real data with some distance measure other than Kullback-Leibler divergence, LFOICA can efficiently learn the mixing matrix via backpropagation. We further demonstrated how LFOICA can be extended to solve a number of causal discovery problems that essentially involve confounders, such as causal discovery from measurement error-contaminated data and low-resolution time series data. Experimental results show that our LFOICA and its extensions enjoy accurate and efficient learning. Compared to previous ones, the resulting causal discovery methods scale much better to rather high-dimensional problems and open the gate to a large number of real applications.

References

- Pearl, J. *Causality: Models, Reasoning, and Inference*; Cambridge University Press: New York, NY, USA, 2000.
- Spirtes, P.; Glymour, C. N.; Scheines, R.; Heckerman, D.; Meek, C.; Cooper, G.; Richardson, T. *Causation, prediction, and search*; MIT press, 2000.
- Chickering, D. M. *Journal of machine learning research* **2002**, *3*, 507–55@articlearjovsky2017wasserstein, title=Wasserstein gan, author=Arjovsky, Martin and Chintala, Soumith and Bottou, Léon, journal=arXiv preprint arXiv:1701.07875, year=2017 4.
- Shimizu, S.; Hoyer, P. O.; Hyvärinen, A.; Kerminen, A. *Journal of Machine Learning Research* **2006**, *7*, 2003–2030.
- Hoyer, P. O.; Janzing, D.; Mooij, J. M.; Peters, J.; Schölkopf, B. Nonlinear causal discovery with additive noise models. NIPS. 2009; pp 689–696.
- Zhang, K.; Hyvärinen, A. On the identifiability of the post-nonlinear causal model. UAI. 2009; pp 647–655.
- Zhang, K.; Gong, M.; Ramsey, J.; Batmanghelich, K.; Spirtes, P.; Glymour, C. Causal Discovery with Linear Non-Gaussian Models under Measurement Error: Structural Identifiability Results. UAI. 2018.
- Hoyer, P. O.; Shimizu, S.; Kerminen, A. J.; Palviainen, M. *International Journal of Approximate Reasoning* **2008**, *49*, 362–378.
- Geiger, P.; Zhang, K.; Schoelkopf, B.; Gong, M.; Janzing, D. Causal inference by identification of vector autoregressive processes with hidden components. ICML. 2015; pp 1917–1925.
- Gong, M.; Zhang, K.; Schoelkopf, B.; Tao, D.; Geiger, P. Discovering temporal causal relations from subsampled data. ICML. 2015; pp 1898–1906.
- Gong, M.; Zhang, K.; Schölkopf, B.; Glymour, C.; Tao, D. Causal discovery from temporally aggregated time series. UAI. 2017.
- Tank, A.; Fox, E. B.; Shojaie, A. *Biometrika* **2019**, *106*, 433–452.
- Hyvärinen, A.; Karhunen, J.; Oja, E. *Independent component analysis*; John Wiley & Sons, 2004; Vol. 46.
- Olshausen, B. A.; Millman, K. J. Learning sparse codes with a mixture-of-Gaussians prior. NIPS. 2000; pp 841–847.

Højen-Sørensen, P. A.; Winther, O.; Hansen, L. K. *Neural Computation* **2002**, *14*, 889–918.

Petersen, K. B.; Winther, O.; Hansen, L. K. *Neural computation* **2005**, *17*, 1921–1926.

Goodfellow, I.; Pouget-Abadie, J.; Mirza, M.; Xu, B.; Warde-Farley, D.; Ozair, S.; Courville, A.; Bengio, Y. Generative adversarial nets. NIPS. 2014; pp 2672–2680.

Kingma, D. P.; Ba, J. *arXiv preprint arXiv:1412.6980* **2014**,

Duchi, J.; Hazan, E.; Singer, Y. *Journal of Machine Learning Research* **2011**, *12*, 2121–2159.

Hyvarinen, A. *IEEE transactions on Neural Networks* **1999**, *10*, 626–634.

Brakel, P.; Bengio, Y. *arXiv preprint arXiv:1710.05050* **2017**,

Amari, S.-i.; Cichocki, A.; Yang, H. H. A new learning algorithm for blind signal separation. NIPS. 1996; pp 757–763.

Hyvärinen, A.; Oja, E. *Neural networks* **2000**, *13*, 411–430.

Le, Q. V.; Karpenko, A.; Ngiam, J.; Ng, A. Y. ICA with reconstruction cost for efficient overcomplete feature learning. NIPS. 2011; pp 1017–1025.

Arjovsky, M.; Chintala, S.; Bottou, L. *arXiv preprint arXiv:1701.07875* **2017**,

Li, Y.; Swersky, K.; Zemel, R. Generative moment matching networks. ICML. 2015; pp 1718–1727.

Gretton, A.; Borgwardt, K. M.; Rasch, M. J.; Schölkopf, B.; Smola, A. *Journal of Machine Learning Research* **2012**, *13*, 723–773.

Sriperumbudur, B. K.; Fukumizu, K.; Lanckriet, G. R. *Journal of Machine Learning Research* **2011**, *12*, 2389–2410.

Eriksson, J.; Koivunen, V. *IEEE signal processing letters* **2004**, *11*, 601–604.

Tibshirani, R. *Journal of the Royal Statistical Society: Series B (Methodological)* **1996**, *58*, 267–288.

Nitanda, A. In *NIPS*; Ghahramani, Z., Welling, M., Cortes, C., Lawrence, N. D., Weinberger, K. Q., Eds.; Curran Associates, Inc., 2014; pp 1574–1582.

Kingma, D. P.; Welling, M. *arXiv preprint arXiv:1312.6114* **2013**,

Jang, E.; Gu, S.; Poole, B. *arXiv preprint arXiv:1611.01144* **2016**,

Maddison, C. J.; Mnih, A.; Teh, Y. W. The Concrete Distribution: A Continuous Relaxation of Discrete Random Variables. ICLR. 2017.

Mirza, M.; Osindero, S. *arXiv preprint arXiv:1411.1784* **2014**,

Sachs, K.; Perez, O.; Pe'er, D.; Lauffenburger, D. A.; Nolan, G. P. *Science* **2005**, *308*, 523–529.

Lacerda, G.; Spirtes, P. L.; Ramsey, J.; Hoyer, P. O. *arXiv preprint arXiv:1206.3273* **2012**,

Mooij, J. M.; Peters, J.; Janzing, D.; Zscheischler, J.; Schölkopf, B. *Journal of Machine Learning Research* **2016**, *17*, 1–102.